Traveling Wave Cylindrical Induction Heating System

Prof. Dr. Jafar Hamid Alwash
Electrical Engineering Department
College of Engineering, University of Baghdad
jalwash@yahoo.com

M.Sc. Riyadh Kamil Chillab
Electrical Engineering Department
College of Engineering, University of Baghdad
inductionm@yahoo.com

ABSTRACT

The paper deals with the traveling wave cylindrical heating systems. The analysis presented is analytical and a multi-layer model using cylindrical geometry is used to obtain the theoretical results.
To validate the theoretical results, a practical model is constructed, tested and the results are compared with the theoretical ones. Comparison showed that the adopted analytical method is efficient in describing the performance of such induction heating systems.

KEY WORDS: induction heating, cylindrical heating systems.

نظام التسخين الحثي الاسطواني ذو الموجة المنتقلة

م.م. رياض كامل جلاب **أ.د. جعفر حميد علوش**

الخلاصة

يوضح هذا البحث الدراسة النظرية و العملية لتحليل أنظمة التسخين الحثي ذات الموجة المتنقلة لقطع معدنية إسطوانية الشكل. تم بناء و تشغيل نموذج عملي لأتمام الفحوصات المختبرية لهذا النوع من المسخنات.
إن الطريقة التي تم إستخدامها نظريا لتحليل هذا المسخن هي طريقة تحليلية صرفة تعرف بنظرية الطبقات المتعددة بإستخدام المحاور الإسطوانية.
تمت المقارنة بين النتائج النظرية و المختبرية، و أظهرت هذه المقارنة كفاءة الطريقة المستخدمة نظريا لإستقراء إداء هذا النوع من المسخنات الحثية.

الكلمات الرئيسية : التسخين الحثي، أنظمة التسخين الاسطواني.

LIST OF PRINCIPAL SYMBOLS

B	magnetic flux density, T
E	electric field strength, V/m
H	magnetic field strength, A/m
k	wave length factor = $2\pi/\lambda$
P_w	power induced in the charge, W
P	number of poles
I_{max}	peak of phase current, A
J'	amplitude of line current density, A
l	axial coil length, m
m	number of phases
N_{eff}	effective number of series turns per phase
Z_t	terminal impedance, Ω
F	supply frequency, Hz
r,θ,z	subscripts for cylindrical coordinates
s	Slip
λ	wavelength of exciting wave, m
μ	permeability, H/m
σ	conductivity, s/m
ω	equal to $2\pi f$

1. INTRODUCTION

The primary object of this work is to propose a general mathematical model for the system Fig.(1) using the actual topology for three-phase excitation with any number of poles in the axial direction. As a second object, the paper employs the multi-layer approach with an appropriate current sheet representation to calculate the flux density

components, induced power in the charge, terminal impedance and electromagnetic force in the direction of the traveling field.

The primary coil construction may be explained in a similar manner with the aid of Fig.(2) which shows the cylindrical windings in its tubular form with multi-polar system distributed axially. The model shown in Fig.(2-a) has two axial poles, and Fig.(2-b) has six axial poles.

2.MATEHMATICAL MODEL

A general multi-region problem is analyzed. The model is taken to be a set of infinitely long concentric cylinders, with a radialy infinitesimally thin and axially infinite current sheet excitation of radius r_g. It is further assumed that magnetic saturation is neglected.

Maxwell's equations for any region in the model are

$$\text{curl } H = J \quad (1)$$

$$\text{curl } E = -\frac{\partial B}{\partial t} \quad (2)$$

$$\text{div } E = 0 \quad (3)$$

$$\text{div } B = 0 \quad (4)$$

$$\text{div } J = 0 \quad (5)$$

$$J = \sigma E \quad (6)$$

$$B = \mu H \quad (7)$$

Assumptions

Maxwell's equations are solved using cylindrical coordinates system subject to the following assumptions and boundary conditions.

1. The induction heating system is infinitely long in the axial z- direction.
2. Displacement currents are considered negligible at the frequencies used.
3. All field quantities decay to zero at sufficiently large radial distances from the induction heating system axis of symmetry.
4. The radial component of flux density (B_r) is continuous across a boundary.
5. The radial component of line current density (J_r) is assumed to be zero.
6. The axial component of magnetic field strength (H_z) is continuous across a boundary, but allowance for the current sheet should be taken into account.
7. Longitudinal end effects are neglected.

3. THEORETICAL ANALYSIS

3.1 The primary current density

The primary winding considered is of cylindrical geometry and the excitation wave produced is assumed to be a perfect sinusoidal traveling wave. The line current density may be represented as

$$J_\theta = Re\left[J' e^{j(\omega t - kz)}\right] \quad (8)$$

Where

$$J' = \frac{4mN_{eff} I_{\max}}{\lambda \cdot P}$$

The field produced will link all regions (1) to (N).

3.2 The field equations of a general region

As a first step in the analysis, the field components of a general region are derived. Assuming that all fields vary as $e^{j(\omega t)-kz}$ [2], and omitting this factor for shortness from all the field expressions that follow.

Taking only the radial component form both sides of equation (2) gives

$$\frac{\partial E_\theta}{\partial z} = j\omega\mu H_r$$

or

$$H_r = -\frac{kE_\theta}{\omega\mu} \quad (9)$$

Taking only the z-component form both sides of equation (2), one can get

$$\frac{1}{r}\frac{\partial r E_\theta}{\partial r} = -j\omega\mu H_z \quad (10)$$

Using equation (1) and (6) and taking only the θ-component from both sides, gives,

$$\frac{\partial H_r}{\partial z} - \frac{\partial H_Z}{\partial r} = \sigma E_\theta \quad (11)$$

After rearranging, equation (11) may be written in the form

$$r^2\frac{\partial^2 E_\theta}{\partial r^2} + r\frac{\partial E_\theta}{\partial r} - \left(\alpha^2 r^2 + 1\right)E_\theta = 0 \quad (12)$$

The solution is given by

$$E_\theta = AI_1(\alpha r) + DK_1(\alpha r) \quad (13)$$

Where

$$\alpha^2 = k^2 + j\omega\mu\sigma$$

and ω is replaced by (sω) for any region with slip s. I_1 and K_1 are the modified Bessel functions of the first order and of general complex argument. A and D are arbitrary constants to be determined from boundary conditions.

Using equations (2), (7) and (13), it can be shown that

$$H_z = j\frac{\alpha}{\omega\mu}\left[AI_0(\alpha r) + DK_0(\alpha r)\right] \qquad (14)$$

3.3 Field calculation at the region boundaries

Fig.(3-a) shows a general region n, where $E_{\theta,n}$ and $H_{z,n}$ are the field components at the upper boundary of the region, and $E_{\theta,n-1}$ and $H_{z,n-1}$ are the equivalent values at the lower boundary.

From equation (13) and (14), it can be shown that

$$E_{\theta,n} = AI_1(\alpha_n r_n) + DK_1(\alpha_n r_n) \qquad (15)$$

and

$$H_{z,n} = j\frac{\alpha_n}{\omega\mu_n}\left[AI_0(\alpha_n r_n) - DK_0(\alpha_n r_n)\right] \qquad (16)$$

Equivalent expressions for $E_{\theta,n-1}$ and $H_{z,n-1}$ can be found by replacing (r_n) in the above expressions by (r_{n-1}).

Now, for regions where n ≠ 1 or N,

$$\begin{bmatrix} E_{\theta,n} \\ H_{z,n} \end{bmatrix} = [T_n] \cdot \begin{bmatrix} E_{\theta,n-1} \\ H_{z,n-1} \end{bmatrix} \qquad (17)$$

Where $[T_n]$ is the transfer matrix [3,4] for region n, and is given by

$$[T_n] = \begin{bmatrix} a_n & b_n \\ c_n & d_n \end{bmatrix} \qquad (18)$$

Expressions for the transfer matrix elements are given in the appendix. Hence, given the values of E_θ and H_z at the lower boundary of a region, the values of E_θ and H_z at the upper boundary can be found using the transfer matrix. At boundaries where no excitation current sheet exists E_θ and H_z are continuous. Thus, for example, if two regions are considered to have no current sheet at their common boundary, knowing the values of E_θ and H_z at the beginning of the first region, values of E_θ and H_z at the end of the second region can be found by successive use of two transfer matrices.

Now, considering the current sheet to be at radius r_g, then

$$H'_{r,n} = H_{z,n} \qquad n \neq g \qquad (19)$$

and

$$H'_{r,n} = H_{z,n} - J' \qquad n = g \qquad (20)$$

Where $H_{z,n}$ is the axial magnetic field strength immediately below a boundary, and $H'_{z,n}$ is the magnetic field strength immediately above a boundary. Bearing in mind the boundary conditions, it is apparent that for the model under consideration, it can be written that

$$\begin{bmatrix} E_{\theta,N-1} \\ H_{z,N-1} \end{bmatrix} = [T_{N-1}] \cdot [T_{N-2}] \cdot \cdots\cdots [T_{g+1}] \begin{bmatrix} E_{\theta,g} \\ H_{z,g} - J' \end{bmatrix} \qquad (21)$$

and

$$\begin{bmatrix} E_{\theta,g} \\ H_{z,g} \end{bmatrix} = [T_g] \cdot [T_{g-1}] \cdot \cdots\cdots [T_2] \begin{bmatrix} E_{\theta,1} \\ H_{z,1} \end{bmatrix} \qquad (22)$$

If region N is now considered, Fig. (3-b), then

$$I_1(\alpha r) \to \infty \text{ as } (r \to \infty).$$

Therefore, from equation (15) and (16) one may obtain that (A=0) and

$$E_{\theta,N-1} = DK_1(\alpha_N r_{N-1}) \qquad (23)$$

and

$$H_{z,N-1} = -j\frac{\alpha_N}{\omega\mu_N} DK_0(\alpha_N r_{N-1}) \qquad (24)$$

Considering the first region (1), then

$$K_1(\alpha r) \to \infty \text{ as } (r \to 0)$$

Therefore, from equation (15) and (16) one may obtain that (D=0) and

$$E_{\theta,1} = AI_1(\alpha_1 r_1) \qquad (25)$$

and

$$H_{z,1} = j\frac{\alpha_1}{\omega\mu_1} A I_0(\alpha_1 r_1) \quad (26)$$

It should be appreciated that equations (23 … 26) describing the field components at the boundaries of regions (1) and (N) still contain arbitrary constants. However, the ratios of E_θ to H_z at these boundaries contain no arbitrary constants, and it is only these ratios that are needed for a complete solution. The next section shows how this may be accomplished. The ratios of E_θ to H_z have been termed the surface impedance [5].

3.4 Surface impedance calculations

The surface impedance looking outwards at a boundary of radius r_s is defined as [6],

$$Z_{s+1} = \frac{E_{\theta,s}}{H'_{z,s}} \quad (27)$$

and the surface impedance looking inwards a boundary is defined as

$$Z_s = -\frac{E_{\theta,s}}{H_{z,s}} \quad (28)$$

Using the method given in [6] with the values of $E_{\theta,N-1}$, $H_{z,N-1}$, $E_{\theta,1}$, $H_{z,1}$ and that of (a_n, b_n, c_n and d_n) as given in the appendix, it can be shown that

$$Z_{in} = \frac{Z_g Z_{g+1}}{Z_g + Z_{g+1}} \quad (29)$$

Where Z_{in} is the input surface impedance at the current sheet, and Z_{g+1} and Z_g are the surface impedances looking outwards and inwards at the current sheet.

Substituting for Z_g and Z_{g+1} using equations (28) and (27) respectively, and with rearranging to get

$$Z_{in} = \frac{-E_{\theta,g}}{H_{z,g} - H'_{z,g}} \quad (30)$$

From equation (20)

$$H'_{z,g} = H_{z,g} - J'$$

Substituting this in equation (30)

$$Z_{in} = \frac{-E_{\theta,g}}{J'} \quad (31)$$

Thus, the input impedance at the current sheet (Z_{in}) has been determined. This means that all the field components can be found by making use of this and equations (28), (21) and (22).

3.5 Terminal impedance

The terminal impedance per phase can be derived in terms of Z_{in} [7], as

$$Z_t = \frac{16 \cdot m \cdot \pi \cdot N_{eff}^2 \cdot r_g \cdot Z_{in}}{\lambda \cdot P} \quad (32)$$

3.6 Power calculations

Having found E_θ and H_z at all boundaries, it is then a simple matter to calculate the power entering a region through the concept of pointing vector. The time average power passing through a surface is given [7], as

$$P_{in} = \frac{1}{2} Re\left(\overline{E}_\theta \times \overline{H}_z^*\right) \quad (\text{w/m}^2) \quad (33)$$

Using equations. (28), (31) and (33), it can be shown that the total charge power is

$$P_w = \frac{1}{2}\left|J'\right|^2 Re(Z_{in})(2\pi r_g l) \quad (\text{w}) \quad (34)$$

3.7 Axial force

It follows that the axial acting force on the region [8] is

$$F_z = \frac{P_w}{\lambda f} \ (\text{N}) \quad (35)$$

4. EXPERIMENTAL MODEL

4.1 Model description

Fig.(4) shows the experimental test rig. The coils (primary winding) were wound circularly on a plastic tube, and held in positions through using circular guides. These guides were fixed on the tube in such away to make ditches between them. These ditches represent the slots of the primary circuit. Since the core has no backing iron then the primary circuit is of the open type. Each slot

(which is open) is filled with a coil, and the coils are connected in star to a variable voltage supply. It is worth mentioning that these star connected coils represent the heating part of the system (heater). The heater was then mounted and fixed on a board using a suitable mechanical structure. This enables fine adjustment for a uniform air-gap surrounding the workpiece that represents the load (charge). The type of the charge used is a solid aluminum cylinder.The magnetic circuit for this material provides the required flux paths. The conductivity of the charge was measured using standard DC measurement. Table 1 shows the parameters of the experimental model.

To calculate the magnetic flux density on the charge surface, simple type of independent probe (search coil) was used. The magnetic flux density in the axial direction was measured using a (B – probe), as will be explained in the next section.

4.2 B – probe

A search coil is used to investigate the axial component of magnetic flux density at different positions on the surface of the charge. Five identical B-probes, displaced (5 cm) from each other, were used to measure the magnitude of the magnetic flux density. Each probe consists of (200) turns of thin wire of size (SWG 30) wound around the cylindrical charge, of ($\pi \cdot r_w^2$) area. The coil ends were twisted together and connected to a digital voltmeter.

Using Faraday's law, the induced voltage V_C across the search coil is

$$V_C = n_c \cdot \omega \cdot A_c \cdot B \qquad (36)$$

Where

r_w : radius of the charge, (mm)

n_c : number of turns of the search coil.

A_c : cross sectional area of the charge around which search coil is wound, (m^2)

4.3 Load power measurement

The load power was measured experimentally as follows:

a. The input power to the heater was measured by using two wattmeter method.

b. Primary phase current was measured using an ammeter. Then, the copper loss for the three-phase primary winding (coils) was calculated, as

$$P_{cs} = 3I_{ph}^2 R_{ph} \quad \text{(w)} \qquad (37)$$

Where

P_{cs} : Copper loss of coil conductors, (w).

I_{ph} : Primary phase current, (A).

R_{ph} : Resistance of primary coil per phase, (Ω)

c. The load power in charge was found by subtracting the copper losses from the input power, as follows

$$P_{ch} = P_t - P_{cs} \quad \text{(w)} \qquad (38)$$

Where

P_{ch} : Load power in charge, (w).

P_t : Total input power, (w).

4.4 Axial force measurement

An experimental measurement of the axial force has been implemented using the experimental set-up shown in Fig.(5). Each point was found, by adjusting the suspended mass (M_z), to balance the force produced by the system. The force is then calculated using the following equation

$$F_z = M_z \times g_a \quad \text{(N)} \qquad (39)$$

Where

F_z : Axial force, (N).

M_z : Mass, (Kg).

g_a : Acceleration of gravity = 9.81 m/sec^2.

5. RESULTS

Theoretical and experimental results were executed with different number of poles. Variable three-phase current excitation was used at a test frequency of 50 Hz.

Fig. (6), and (7) show the variation of charge power with exciting current per phase for 2,and 6 poles respectively.

From the results, it is clear that increasing number of poles reduces the power induced in the charge. This of course is to be expected since increasing the number of poles is accompanied by reducing the effective number of turns per pole per phase.

The layer theory approach has been used for the analysis of induction heating system with rotational symmetry with three-phase excitation. The analysis presented is quite general in that it lends itself to the analysis of traveling wave induction heating systems with any number of poles.

The displayed results show clearly that the theoretical results correlate well with the experimental ones. This may be considered as fair justification to the method adopted for the analysis in this work.

6. Conclusions

The layer theory approach has been used for the analysis of induction heating system with rotational symmetry with three-phase excitation. The analysis presented is quite general in that it lends itself to the analysis of traveling wave induction heating systems with any number of poles.

The displayed results show clearly that the theoretical results correlate well with the experimental ones. This may be considered as fair justification to the method adopted for the analysis in this work

7. Appendixes

7.1 Transverse matrix elements

$$a_n = \alpha_n r_{n-1}\left[I_1(\alpha_n r_n)K_0(\alpha_n r_{n-1}) + I_0(\alpha_n r_{n-1})K_1(\alpha_n r_n)\right] \quad (40)$$

$$b_n = j\omega\mu_n r_{n-1}\left[I_1(\alpha_n r_{n-1})K_1(\alpha_n r_n) - I_1(\alpha_n r_n)K_1(\alpha_n r_{n-1})\right] \quad (41)$$

$$c_n = j\frac{\alpha_n^2 r_{n-1}}{\omega\mu_n}\left[I_0(\alpha_n r_n)K_0(\alpha_n r_{n-1}) - I_0(\alpha_n r_{n-1})K_0(\alpha_n r_n)\right] \quad (42)$$

$$d_n = \alpha_n r_{n-1}\left[I_0(\alpha_n r_n)K_1(\alpha_n r_{n-1}) + I_1(\alpha_n r_{n-1})K_0(\alpha_n r_n)\right] \quad (43)$$

REFERENCES

- Freeman, E.M., and Smith, B. E.; “Surface impedance method applied to multilayer cylindrical induction devices with circumferential exciting currents”; Proc. IEE, vol. 117, No. 10, pp 2012-2013, Oct. 1970.
- Alwash, J. H.; “Analysis and Design of Linear Induction Machines”; Ph.D. Thesis, Imperial College, London University, U. K., 1972.
- Greig, J., and Freeman, E.M.; “Traveling wave problem in electrical machine”; Proc. IEE, vol. 114, pp. 1681-1683, Nov. 1967.
- Freeman, E.M.; “Traveling waves in induction machines: input impedance and equivalent circuits”; Proc. IEE, vol. 115, No. 12, pp. 1772-1776, Dec. 1968.
- J. H. H. Alwash, A. D. Muhsen and A. S. Abdi; “Helical motion tubular induction motor”; IEEE Trans. Energy Conv., vol. 18, No. 3, pp. 362-369, Sep. 2003.
- Eastham, J. F., and Alwash, J. H.; “Transverse-flux tubular motors”; Proc. IEE, vol. 119, No. 12, pp. 1709-1718, Des. 1972.
- Mohssen, A. D.; ”Predicting the performance of helical winding induction motors”; M.Sc. Thesis, College Engineering, Baghdad University, Baghdad 1996.
- Al-shammari, R. K.; "Analysis of traveling wave cylindrical induction heating systems”; M.Sc. Thesis, Elect. Eng. Dept., College of Engineering, University of Baghdad, 2009.

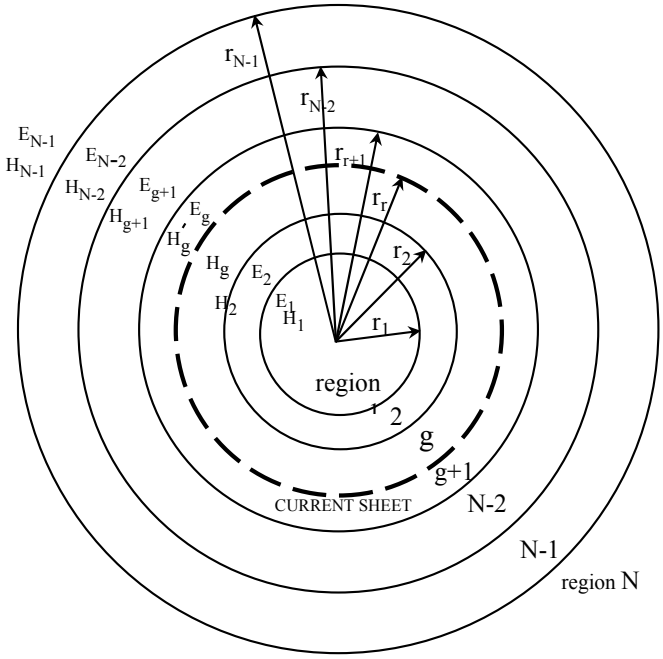

Fig.(1)
Cross-sectional view through multi-cylindrical induction heating system

(a) **(b)**

Fig.(2): Three-phase windings form of induction heater with different number of poles
(a) 2-poles connection (b) 6-poles connection

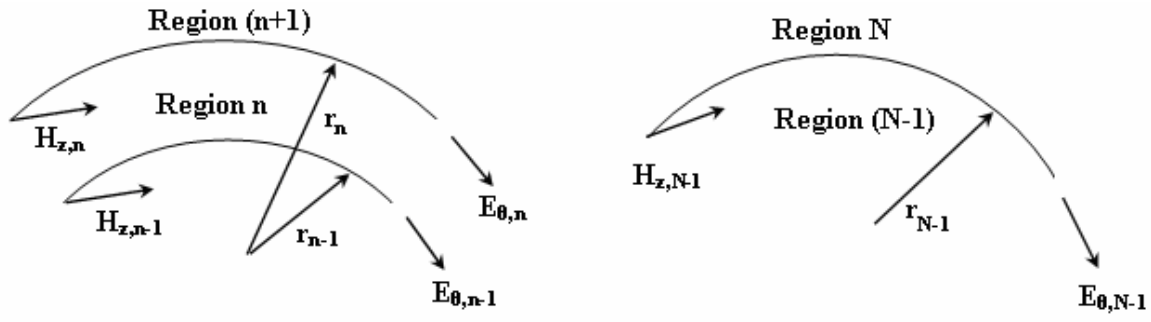

(a) **(b)**

Fig.(3): Mathematical model
(a) General region n (b) End region N

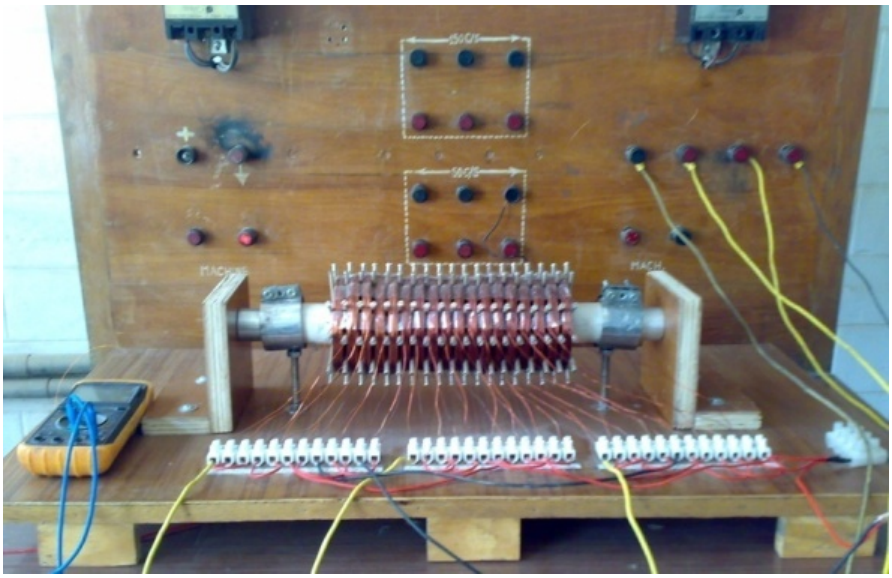

Fig.(4)
Photograph of the experimental model

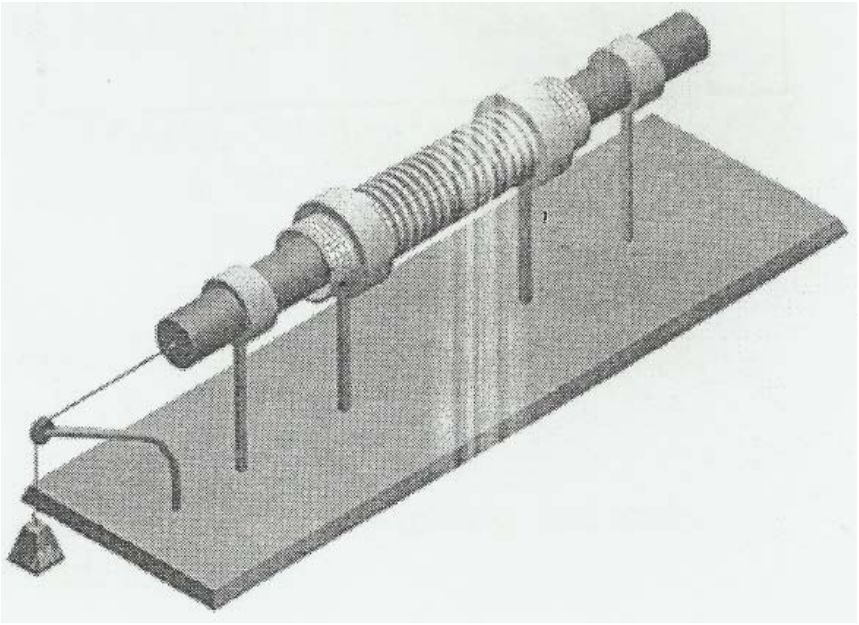

Fig.(5)
Experimental set-up for measuring the axial force

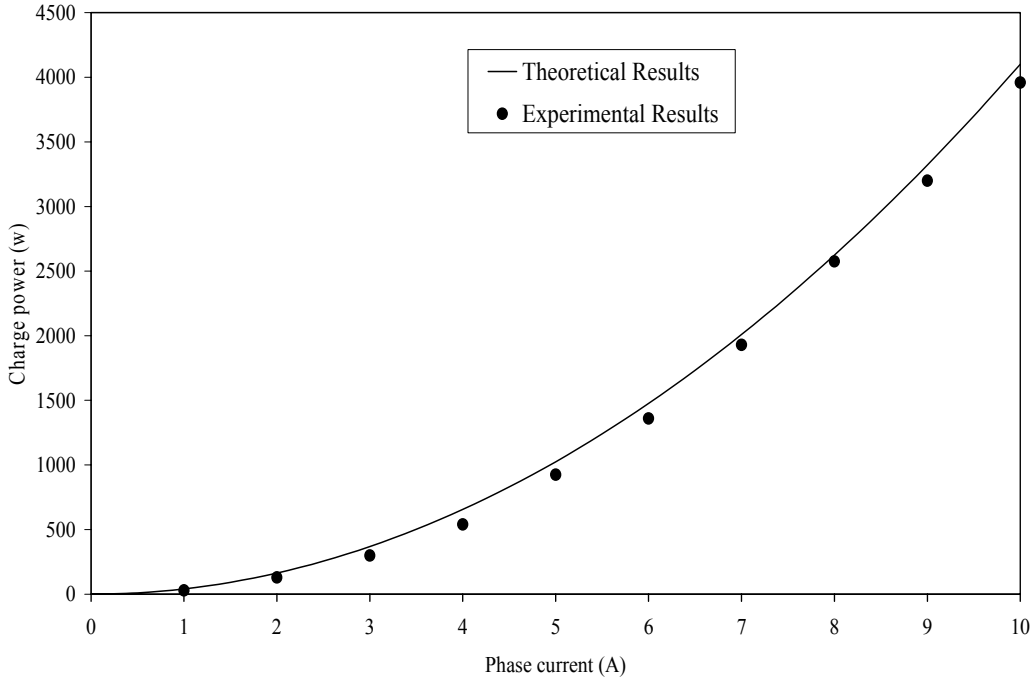

Fig.(6)
Variation of charge power with phase current (2-pole connection)

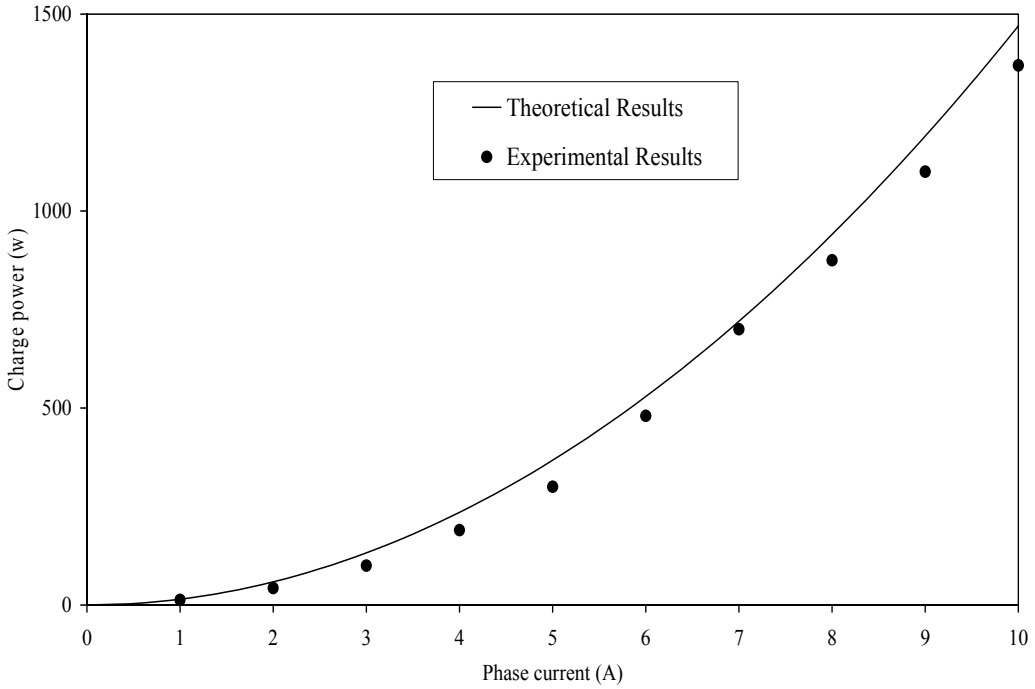

Fig.(7)
Variation of charge power with phase current (6-pole connection)

Table 1
Experimental model parameters

Parameter/Characteristic	Value
Phases	3
Axial poles	2,6
Number of slots (coils)	18
Turns per coil	260
Coil inner diameter (mm)	50
Slot width (mm)	10
Slot pitch (mm)	16
Slot depth (mm)	37
Frequency (Hz)	50
Air-gap length (mm)	5
Primary conductor wire gauge	SWG 19.5
Charge length (mm)	294
Charge radius (mm)	20
Charge conductivity (s/m)	3.4×10^{7}
Charge relative permeability	1
Exciting phase current (A)	Variable